Dalton Transactions

ROYAL SOCIETY OF CHEMISTRY

PAPER

View Article Online
View Journal | View Issue

Cite this: *Dalton Trans.*, 2026, **55**, 3733

Synthesis, structures and catalytic properties of two organic–inorganic hybrid polyoxometalates built from {Ni_6PW_9} units

Shuang Gao,[a,b] Zhen-Wen Wang[b] and Guo-Yu Yang *[b]

Received 19th December 2025,
Accepted 2nd February 2026

DOI: 10.1039/d5dt03040d

rsc.li/dalton

Two new Ni_6-added organic–inorganic hybrid polyoxometalates, {$[Ni(en)_2][Ni_6(\mu_3\text{-}OH)_3(H_2O)_3(Hen)(en)_3(3,5\text{-}DDB)(B\text{-}\alpha\text{-}PW_9O_{34})][Ni_6(\mu_3\text{-}OH)_3(H_2O)_2(en)_3(Ac)(3,5\text{-}DDB)(B\text{-}\alpha\text{-}PW_9O_{34})]\}\cdot 8H_2O$ (**1**, en = ethylenediamine, 3,5-DDB = 3,5-dihydroxybenzoic acid) and $[Ni(en)_2][Ni_6(\mu_3\text{-}OH)_3(H_2O)_4(en)_2(5\text{-}HIP)(B\text{-}\alpha\text{-}PW_9O_{34})]\cdot 3H_2O$ (**2**, 5-HIP = 5-hydroxyisophthalic acid), were synthesized using a lacunary-directing synthetic strategy. **1** forms a novel dumbbell-shaped dimer structure consisting of two distinct Ni_6-added POMs linked by $[Ni(en)_2]^{2+}$ cations. **2** exhibits a one-dimensional (1D) chain structure assembled from $[Ni_6(\mu_3\text{-}OH)_3(H_2O)_4(en)_2(B\text{-}\alpha\text{-}PW_9O_{34})]^{2-}$ structural building units bridged by 5-HIP ligands. Electrochemical studies revealed that **1** exhibits significant electrocatalytic activity for the reduction of H_2O_2 and NO_2^-. Furthermore, evaluation experiments on oxidative desulfurization revealed that complex **2** exhibits a higher desulfurization conversion rate for dibenzothiophene (DBT) compared to complex **1**. Additionally, it was observed that increasing both the reaction temperature and the amount of H_2O_2 further improved the desulfurization efficiency of DBT.

Introduction

Polyoxometalates (POMs), a class of nanoscale metal–oxo clusters with well-defined structures, tunable electronic properties, and excellent redox activity, have attracted sustained research interest due to their broad application potential in catalysis, energy conversion, environmental protection, and biomedicine.[1–15] Over the past two decades, lacunary POM precursors derived from Keggin-type POMs have served as ideal templates for constructing transition-metal-added POMs (TMAPs) with precise structures and tailored functionalities.[16–20] These lacunary species offer unique advantages in terms of exposed coordination sites and spatial configurations, enabling the efficient incorporation of various TM ions. TMAPs not only retain the desirable properties of conventional POMs but also exhibit enhanced capabilities in magnetochemistry, catalysis, and photo-electronics due to the introduction of magnetic metal centers.[21–25] Despite these prospects, early studies on hydrothermal synthesis of TMAPs reported considerable challenges, including poor cluster stability, unpredictable metal coordination modes, and difficulties in controlling crystallization.[26,27] Since 2007, our research group has developed a lacunary-directing synthetic (LDS) strategy[28] for the directed assembly of nickel ions with lacunary Keggin units $[XW_9O_{34}]^{n-}$ (X = P, Si, Ge), leading to the successful preparation of a series of Ni_6-added POMs (Ni_6APs) based on the {$Ni_6(\mu_3\text{-}OH)_3(L)(B\text{-}\alpha\text{-}XW_9O_{34})$} building block.[2,28–33] These structures demonstrated remarkable coordinative versatility and structural rigidity, providing a robust foundation for further functionalization.

Inspired by this pioneering work, research attention has increasingly turned toward the organic functionalization of TMAPs. Introducing organic ligands *via* covalent modification or coordination-driven strategies not only modulates the electronic structure and solubility of POMs but also endows them with new functions, greatly expanding their applications in hybrid materials, molecular devices, and asymmetric catalysis.[34,35] Currently, research in this field primarily focuses on two directions: one involves substituting the terminal oxygen sites of POMs with organic groups[36–39] and the other entails employing POMs as secondary building units (SBUs) to construct POM cluster–organic frameworks (POMCOFs) *via* coordination-driven self-assembly with organometallic units or functional organic molecules.[40–42] POMs continue to garner extensive attention in the realms of covalent and coordinative modification. Through the judicious selection of linkers, POMCOFs or molecular cage architectures can be controllably assembled. Consequently, the precise regulation of POMCOFs *via* linker design retains substantial research value.

[a]*Liaoning Key Laboratory of Chemical Additive Synthesis and Separation, Yingkou Institute of Technology, Yingkou 115014, China*
[b]*MOE Key Laboratory of Cluster Science, School of Chemistry and Chemical Engineering, Beijing Institute of Technology, Beijing 100081, China.*
E-mail: ygy@bit.edu.cn, ygy@fjirsm.ac.cn

In this work, based on the LDS strategy, the construction of TMAPs from 0D to 1D chain structures was successfully achieved by introducing single-linker ligands (monocarboxylic acids) and dual-linker ligands (dicarboxylic acids) (Scheme 1). Two new Ni_6-added organic–inorganic hybrid POMs, $\{[Ni(en)_2][Ni_6(\mu_3\text{-}OH)_3(H_2O)_3(Hen)(en)_3(3,5\text{-}DDB)(B\text{-}\alpha\text{-}PW_9O_{34})][Ni_6(\mu_3\text{-}OH)_3(H_2O)_2(en)_3(Ac)(3,5\text{-}DDB)(B\text{-}\alpha\text{-}PW_9O_{34})]\}\cdot 8H_2O$ (**1**) and $[Ni(en)_2][Ni_6(\mu_3\text{-}OH)_3(H_2O)_4(en)_2(5\text{-}HIP)(B\text{-}\alpha\text{-}PW_9O_{34})]\cdot 3H_2O$ (**2**), were synthesized hydrothermally and characterized by FT-IR, PXRD, thermogravimetric analysis, and single-crystal X-ray diffraction (SCXRD). **1** represents a novel dimer consisting of two unique Ni_6AP units interconnected by $[Ni(en)_2]^{2+}$ cations. Complex **2** features a 1D chain structure assembled from $[Ni_6(\mu_3\text{-}OH)_3(H_2O)_4(en)_2(B\text{-}\alpha\text{-}PW_9O_{34})]^{2-}$ units bridged by 5-HIP ligands. Electrocatalytic studies showed that complex **1** exhibits significant activity toward the reduction of H_2O_2 and $NaNO_2$. Furthermore, oxidative desulfurization evaluation revealed that complex **2** achieves a higher conversion rate for DBT than complex **1**. It was also observed that increasing both the reaction temperature and the amount of H_2O_2 further enhanced the desulfurization efficiency of DBT.

Experimental

Materials and methods

The starting material $Na_9[A\text{-}\alpha\text{-}PW_9O_{34}]\cdot 7H_2O$ ($\{PW_9\}$) was synthesized according to the literature.[43] All other chemicals were of reagent grade and used as purchased without further purification. The infrared spectra of KBr tablets (KBr pellets) in the range of 4000–400 cm^{-1} were recorded on a Smart Omni-Transmission spectrometer. Thermogravimetric analysis (TGA) was performed on a Mettler TGA/SDTA 851 thermal analyzer under an air flow atmosphere at a heating rate of 10 °C min^{-1} and a temperature range of 30–1000 °C. Powder X-ray diffraction (PXRD) was performed using a Philips X'Pert-MPD diffractometer with Cu K_α radiation (λ = 1.54056 Å). Electrochemical measurements were performed using the CHI760E electrochemical workstation (Shanghai Chenhua Instrument Co., Ltd, China).

Synthesis of 1

A mixture of $NiCl_2\cdot 6H_2O$ (0.80 g, 3.37 mmol), $\{PW_9\}$ (0.30 g, 0.117 mmol), en (0.3 mL), NaAc/HAc buffer (10 mL, 0.5 M, pH = 4.8) and an appropriate amount of 3,5-DDB was stirred for 2 h, sealed in a 25 mL Teflon-lined stainless-steel autoclave, heated at 175 °C for 5 days and then cooled to room temperature automatically. Green needle-shaped crystals were obtained by filtration, washed with distilled water and dried in air. Yield: 53% (based on $\{PW_9\}$). Elemental analysis (%), calcd for $C_{34}H_{117}N_{18}Ni_{13}O_{97}P_2W_{18}$: C, 6.32; H, 1.82; N, 3.90. Found: C, 6.12; H, 1.67; N, 3.57. FT-IR (KBr pellet, cm^{-1}): 1556 (m), 1367 (m), 1033 (s), 939 (s), 848 (s), 790 (s), 709 (s) (Fig. S1).

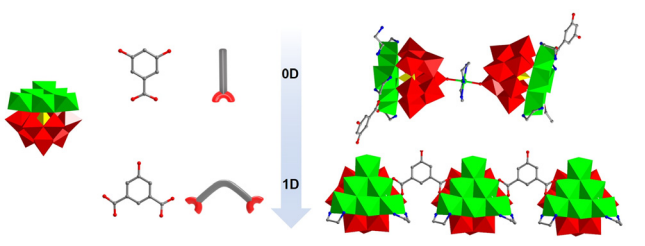

Scheme 1 Lacunary-directing synthesis of TMAPs: from 0D clusters to 1D chains using mono/dicarboxylic acid linkers.

Synthesis of 2

2 was obtained by employing a similar procedure to that for **1** except that 3,5-dihydroxybenzoic acid was replaced by the same mass of 5-HIP. Yield: 41% (based on $\{PW_9\}$). Elemental analysis (%), calcd for $C_{16}H_{53}N_8Ni_7O_{49}PW_9$ (%): C, 5.94; H, 1.65; N, 3.46. Found: C, 6.07; H, 1.67; N, 3.59. FT-IR (KBr pellet, cm^{-1}): 1556 (m), 1384 (m), 1032 (s), 939 (s), 848 (s), 784 (s), 711 (s) (Fig. S1).

X-ray crystallography

The intensity data for **1** and **2** were obtained on a Gemini A Ultra-diffractometer using graphite-monochromated Cu K_α (λ = 1.54056 Å) and Mo K_α (λ = 0.71073 Å) radiation at 293(2) K. The structures were solved by intrinsic phasing using the SHELXT program package[44] and refined using the XL program package[45] by least-squares minimization. All non-hydrogen atoms were refined anisotropically. Crystallographic data have been deposited at the Cambridge Crystallographic Data Centre: 2403241 for **1** and 2404218 for **2**. Crystallographic data and structural refinements are listed in Table 1.

Table 1 Crystallographic data and structural refinements of **1** and **2**

Compound	**1**	**2**
Formula	$C_{34}H_{117}N_{18}Ni_{13}O_{97}P_2W_{18}$	$C_{16}H_{53}N_8Ni_7O_{49}PW_9$
M_r	6464.41	3237.99
Crystal system	Monoclinic	Orthorhombic
Space group	$P2_1/c$	$P2_12_12_1$
T (K)	293(2)	293(2)
a (Å)	21.8358(1)	13.4167(12)
b (Å)	18.1575(1)	13.7245(18)
c (Å)	31.8458(2)	35.498(5)
α (°)	90	90
β (°)	90.5520(10)	90
γ (°)	90	90
V (Å^3)	12 625.75(12)	6536.5(14)
Z	4	4
D_c (Mg m^{-3})	3.381	3.2373
μ (mm^{-1})	32.592	17.854
F(000)	11 664.0	5828.0
Data/restraints/parameters	25 787/962/1641	16 247/5790/801
GOF on F^2	1.042	0.982
Final R indices $[I > 2\sigma(I)]^a$	R_1 = 0.0400, wR_2 = 0.1109	R_1 = 0.0665, wR_2 = 0.1171
R indices [all data]^a	R_1 = 0.0453, wR_2 = 0.1145	R_1 = 0.1465, wR_2 = 0.1497
CCDC number	2403241	2404218

^{a} $R_1 = \sum||F_o| - |F_c||/\sum|F_o|$. w$R_2 = [\sum w(F_o^2 - F_c^2)^2/\sum w(F_o^2)^2]^{1/2}$.

Results and discussion

Structural description

The experimental PXRD patterns of the bulk products **1** and **2** are in good agreement with the simulated PXRD patterns from SCXRD, indicating the high phase purity of the samples (Fig. S2a/b). SCXRD analysis reveals that **1** crystallizes in the monoclinic space group $P2_1/c$ and its asymmetric unit consists of one $[Ni_6(\mu_3\text{-}OH)_3(H_2O)_3(Hen)(en)_3(3,5\text{-}DDB)(B\text{-}\alpha\text{-}PW_9O_{34})]$ (**1A**) cluster, one $[Ni_6(\mu_3\text{-}OH)_3(H_2O)_2(en)_3(Ac)(3,5\text{-}DDB)(B\text{-}\alpha\text{-}PW_9O_{34})]^{2-}$ (**1B**) cluster, one $[Ni(en)_2]^{2+}$ cation, and 8 lattice water molecules (Fig. 1a and S3a). Compared with the typical $\{Ni_6(\mu_3\text{-}OH)_3(H_2O)_6(en)_3\ (B\text{-}\alpha\text{-}PW_9O_{34})\}$ unit,[27] four coordinated water molecules were substituted by 3,5-DDB and an en ligand in **1A** (Fig. 1c), and three coordinated water molecules were substituted by 3,5-DDB and an Ac ligand in **1B** (Fig. 1d). It is noteworthy that **1A** and **1B** are functionalized with two distinct types of organic ligands, a rarity in the realm of POMs. In **1A**, en exhibits two coordination modes: coordination through one nitrogen atom and through two nitrogen atoms, displaying distinct conformations (Fig. S4a/b/c). Interestingly, **1A** and **1B** are connected *via* $[Ni(en)_2]^{2+}$ (Fig. 1b) to form a dimeric structure. Unlike previous polymeric structures, where connectivity typically occurs through terminal oxygen (W=O) with Ni–oxo clusters, in this structure, the terminal oxygen (W=O) coordinates with $[Ni(en)_2]^{2+}$, forming two back-to-back dumbbell-shaped dimeric structures (Fig. 1c and 3d).

Different from **1**, **2** crystallizes in the orthorhombic space group $P2_12_12_1$, and the asymmetric unit of **2** consists of a $[Ni_6(\mu_3\text{-}OH)_3(H_2O)_4\ (en)_2(B\text{-}\alpha\text{-}PW_9O_{34})]^{2-}$ unit, a 5-HIP bridging ligand, an isolated $[Ni(en)_2]^{2+}$ cation and three water molecules (Fig. S3b). Furthermore, $[Ni(en)_2]^{2+}$ in **2** exists outside the framework in a four-coordinate manner, which differs from the six-coordinate $[NiO_2(en)_2]^{2-}$ of **1** (Fig. S5a/b). The coordination modes of $\{Ni_6PW_9\}$ and the 5-HIP are shown in Fig. 2a/b. One $\{Ni_6PW_9\}$ unit connects two 5-HIP linkers, and the 1,3-carboxyls of the 5-HIP linker bind with two $\{Ni_6PW_9\}$ units in an $\eta^1{:}\eta^1{:}\mu_2$ mode. Each $\{Ni_6PW_9\}$ unit is linked to two same ones by μ_2-O (38, 39, 40, 41) atoms to form a 1-D $\{Ni_6PW_9\}_n$ chain (Fig. 3c/e).

This arrangement shares similarities with the 1-D chain of $[Ni(en)_2][Ni_6(en)_3(\mu_3\text{-}OH)_3(1,3\text{-}bdc)(H_2O)_2(B\text{-}\alpha\text{-}PW_9O_{34})]$, where the 1,3-bdc ligands are replaced by 5-HIP. Additionally, it resembles another 1-D chain, $[Ni_6(Hen)(en)_3(OH)_3(Htda)(H_2O)(B\text{-}\alpha\text{-}PW_9O_{34})]$, made of $\{Ni_6PW_9\}$ SBUs and Htda linkers.[30]

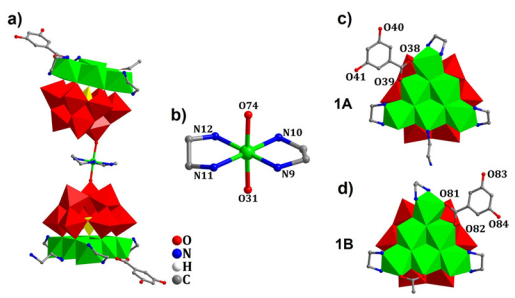

Fig. 1 (a) Polyhedral/ball-and-stick view of **1**; (b) ball-and-stick view of $[Ni(en)_2]^{2+}$; polyhedral/ball-and-stick view of **1A** (c) and **1B** (d).

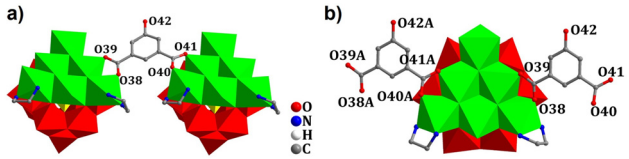

Fig. 2 (a) Coordination environment of the 5-HIP linker, and (b) coordination mode between the $\{Ni_6PW_9\}$ cluster and 5-HIP linkers in **2**. Symmetry code: A (−1 + *x*, *y*, *z*); color codes: red, WO_6; green, NiO_6; and yellow, PO_4.

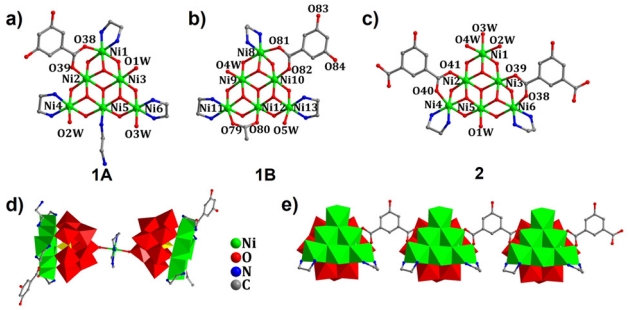

Fig. 3 The coordination environments around **1A**-$\{Ni_6\}$ (a), **1B**-$\{Ni_6\}$ (b) and **2**-$\{Ni_6\}$ (c); polyhedral view of the dumbbell-shaped compound **1** (d), and polyhedral view of the 1D chain compound **2** (e).

Electrochemical properties

The electrochemical and electrocatalytic properties of **1**-CPE were studied in 0.1 M H_2SO_4 + 0.5 M Na_2SO_4 buffer solution at a scan rate of 100 mV s^{-1}. As shown in Fig. 4a, the cyclic voltammogram (CV) of **1** displays two pairs of redox peaks I(−0.328 V)/I′(−0.411 V) and II(−0.579 V)/II′(−0.629 V), and the average peak potentials ($E_{1/2}$) are located at −0.534 V(I/I′) and −0.604 V(II/II′). These two pairs of redox peaks are derived from the redox processes of the W centers in the $[B\text{-}\alpha\text{-}PW_9O_{34}]^{9-}$ fragments. In order to study the influence of the scan speed on CV behavior, CVs of **1**-CPE with different scan speeds (20–500 mV s^{-1}) were tested (Fig. 4b), which reveals that the redox process of **1**-CPE is surface-controlled (Fig. S6).

As is known, some TMAPs can be used as electrocatalysts to catalyze the reduction of H_2O_2 and NO_2^-. In this work, we also investigated the electrocatalytic activity of **1**-CPE toward the reduction of H_2O_2 and NO_2^-. As can be seen from Fig. 4c/d, for **1**-CPE, with the addition of H_2O_2 and NO_2^-, both the reduction peak currents increase gradually, and the corresponding oxidation peak currents decrease, suggesting that the reduction of H_2O_2 and NO_2^- is electrocatalyzed by the reduced species of POMs in **1**.

Oxidative desulfurization

In the evaluation experiment of oxidative desulfurization performance, we systematically investigated the desulfurization

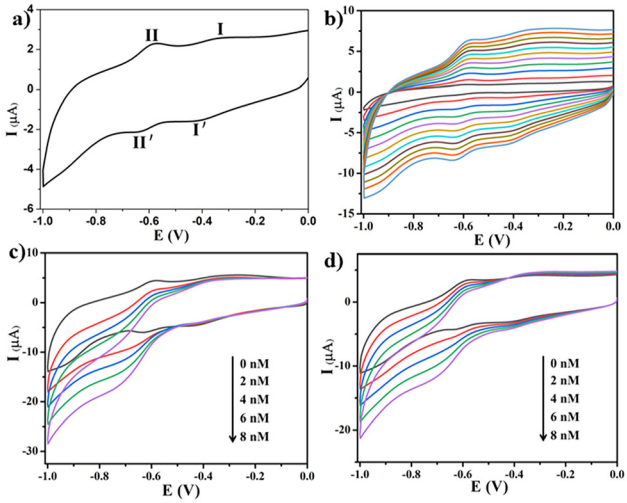

Fig. 4 (a) CV of **1**-CPE in 0.1 M H_2SO_4 + 0.5 M Na_2SO_4 solution. Scan speed: 100 mV s^{-1}. (b) CVs of **1**-CPE at variable scan speeds (20, 50, 100, 150, 200, 250, 300, 350, 400, 450, 500 mV s^{-1}). (c and d) The variation of CVs of **1**-CPE in 0.1M H_2SO_4 + 0.5 M Na_2SO_4 solution with different amounts of H_2O_2 (0, 2, 4, 6, and 8 nM) and KNO_2 (0, 2, 4, 6, and 8 nM). Scan speed: 100 mV s^{-1}.

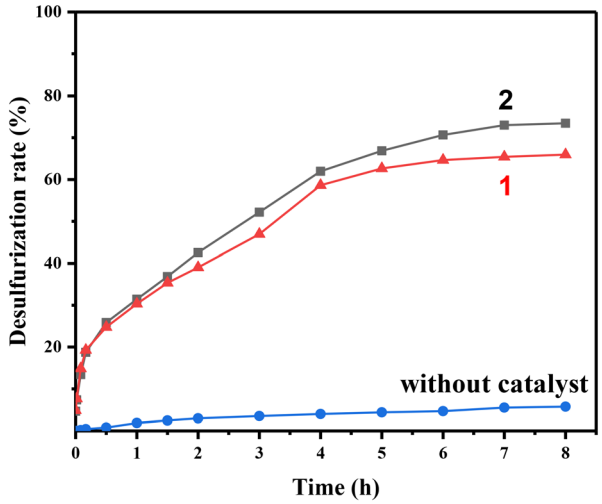

Fig. 5 Oxidative desulfurization performance of compounds **1** and **2**. Reaction conditions: oxidant/oil volume ratio = 2 : 1, T = 60 °C, t = 8 h.

behavior of two POM-based materials under specific reaction conditions (Scheme 2). As shown in Fig. S7, at a reaction temperature of 60 °C, the desulfurization conversion was measured. After 8 hours of reaction, the conversion rate of DBT reached 29.92% for **1**, while it was 36.83% for **2** under the same duration. These results indicate that, at 60 °C and a simulated oil sulfur concentration of 1000 ppm, **2** exhibits higher desulfurization efficiency than **1**. Under the conditions presented in Fig. S8, where the reaction temperature was increased to 80 °C, the desulfurization conversion after 8 hours was 43.46% for **1** and 47.86% for **2**. This further demonstrates the superior performance of **2** under identical sulfur content conditions. It is also observed that within a certain range, increasing the reaction temperature enhances the catalytic activity, thereby improving the desulfurization conversion. As can be seen from Fig. 5, when the reaction temperature was 60 °C, increasing the amount of hydrogen peroxide led to a desulfurization conversion of 73.45% for **2** after 8 hours, while under the same conditions, **1** achieved 65.95% conversion. Once again, **2** showed better desulfurization performance. Furthermore, it can be concluded that at 60 °C, appropriately increasing the molar ratio of hydrogen peroxide to DBT contributes to a further enhancement of the desulfurization conversion.

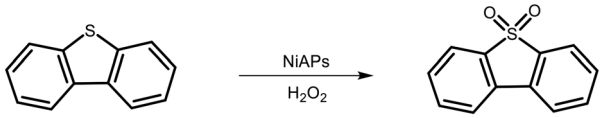

Scheme 2 Oxidative desulfurization reaction.

Conclusions

In summary, compounds **1** and **2** are functionalized with different organic ligands, based on the $\{PW_9O_{34}\}$ unit, forming novel Ni_6AP structures. **1** features a dimer, while **2** possesses a 1D chain. **1** demonstrated good electrocatalytic activity towards the reduction of H_2O_2 and NO_2^- in an acidic medium. In simulated oil desulfurization experiments, the desulfurization efficiency of **2** was consistently higher than that of **1**. Increasing the reaction temperature and the amount of H_2O_2 significantly improved the desulfurization conversion, indicating the potential application of this type of material in fuel desulfurization.

Author contributions

Shuang Gao: conceptualization, methodology, investigation, writing – original draft. Zhen-Wen Wang: formal analysis, validation, writing – review & editing. Guo-Yu Yang: supervision, resources, project administration, writing – review & editing.

Conflicts of interest

The authors declare that they have no known competing financial interests or personal relationships that could have appeared to influence the work reported in this paper.

Data availability

The data supporting the findings of this study are available within the article and its supplementary information (SI). Supplementary information: experimental section, additional

structural information, IR spectra, PXRD patterns, TGA data, and CIF files. See DOI: https://doi.org/10.1039/d5dt03040d.

Any further inquiries may be directed to the corresponding author.

CCDC 2403241 (**1**) and 2404218 (**2**) contain the supplementary crystallographic data for this paper.[46a,b]

Acknowledgements

This work was funded by the National Natural Science Foundation of China (No. 21831001, 21571016, 91122028, and 20725101), the Joint Fund of Liaoning Provincial Natural Science Foundation (2023-MSLH-322), the Foundation of Liaoning Key Laboratory of Chemical Additive Synthesis and Separation (ZJNK2413), and the Yingkou Talent Plan Project-Young Talents (YKYCQB202507).

References

1 J. Liu, N. Jiang, J. M. Lin, Z. B. Mei, L. Z. Dong, Y. Kuang, J. J. Liu, S. J. Yao, S. L. Li and Y. Q. Lan, *Angew. Chem., Int. Ed.*, 2023, **62**, e202304728.
2 S. T. Zheng and G. Y. Yang, *Chem. Soc. Rev.*, 2012, **41**, 7623.
3 S. S. Wang and G. Y. Yang, *Chem. Rev.*, 2015, **115**, 4893.
4 Z. W. Guo, Y. H. Yan, Y. Chen, Y. Y. Li, X. X. Li, C. Sun and S. T. Zheng, *Nat. Commun.*, 2025, **16**, 6379.
5 L. Yang, Z. Zhang, C. N. Zhang and X. L. Wang, *Rare Met.*, 2024, **43**, 236.
6 Z. Li, H. Li, Y. Lin, W. Shi and X. Wang, *J. Am. Chem. Soc.*, 2024, **146**, 28874–28884.
7 H. Z. Wang, Y. Liu, Z. Lin, S. X. Li and G. P. Yang, *Dalton Trans.*, 2026, **55**, 1646–1652.
8 D. He, T. Li, L. Jiang, F. Wang, Z. Xing, N. Wang, Z. Jia and G. Y. Yang, *Nano Res.*, 2024, **17**, 7061–7067.
9 Z. Li, X. Liu, M. Zhao, H. Lv and G. Y. Yang, *Dalton Trans.*, 2025, **54**, 13851–13858.
10 H. L. Guo, X. X. Xing, S. X. Mao, T. Feng, Y. H. Fan, Z. J. Qin, J. Y. Pang, Y. Bai and D. B. Dang, *Dalton Trans.*, 2022, **51**, 18090–18098.
11 G. Dai, Q. Li, D. Zang and Y. Wei, *Green Chem.*, 2023, **25**, 6263–6269.
12 K. Li, Y. Liu, G. Yang, Z. Zheng, X. Lin, Z. Zhang, S. Li, Y. Liu and Y. Wei, *Green Chem.*, 2024, **26**, 6454–6460.
13 J. Wang, H. Yu, Z. Wei, Q. Li, W. Xuan and Y. Wei, *Research*, 2020, 3875920.
14 K. Chen, A. Bayaguud, H. Li, Y. Chu, H. Zhang, H. Jia, B. Zhang, Z. Xiao, P. Wu, T. Liu and Y. Wei, *Nano Res.*, 2018, **11**, 1313–1321.
15 Y. H. Dong, Q. H. Zhou, R. T. Liu, Y. J. Song, S. Y. Huang, J. Y. Pang, D. B. Dang and Y. Bai, *Polyoxometalates*, 2025, **4**, 9140099.
16 C. Schroden, C. F. Blanford, B. J. Melde, B. J. S. Johnson and A. Stein, *Chem. Mater.*, 2001, **13**, 1074.
17 I. Bar-Nahum and R. Neumann, *Chem. Commun.*, 2003, **39**, 2690.
18 F. Odobel, M. Severac, Y. Pellegrin, E. Blart, C. Fosse, C. Cannizzo, C. R. Mayer, K. J. Eliott and A. Harriman, *Chem. – Eur. J.*, 2009, **15**, 3130.
19 P. R. Marcoux, B. Hasenknopf, J. Vaissermann and P. Gouzerh, *Eur. J. Inorg. Chem.*, 2003, **13**, 2406.
20 Q. Chen, D. P. Goshorn, C. P. Scholes, X.-L. Tan and J. Zubieta, *J. Am. Chem. Soc.*, 1992, **114**, 4667.
21 J. L. Zhou, X. Y. Xiang, L. T. Xu, J. L. Wang, S. M. Li, Y. T. Yu, H. Mei and Y. Xu, *Dalton Trans.*, 2023, **52**, 9465–9471.
22 Z. L. Lang, J. Miao, H. Q. Tan, Z. M. Su, Y. G. Li and Z. P. Zheng, *Inorg. Chem. Front.*, 2020, **7**, 4507–4516.
23 E. Tanuhadi, J. Cano, S. Batool, A. Cherevan, D. Eder and A. Rompel, *J. Mater. Chem. C*, 2022, **10**, 17048–17052.
24 L. Z. Han, C. Q. Jiao, W. C. Chen, K. Z. Shao, L. Y. Jin and Z. M. Su, *Dalton Trans.*, 2021, **50**, 11535–11541.
25 Z. Zhang, Y. L. Wang, Y. Liu, S. L. Huang and G. Y. Yang, *Nanoscale*, 2020, **12**, 18333–18341.
26 O. Oms, A. Dolbecq and P. Mialane, *Chem. Soc. Rev.*, 2012, **41**, 7497.
27 P. Mialane, A. Dolbecq and F. Sécheresse, *Chem. Commun.*, 2006, **42**, 3477.
28 S. T. Zheng, D. Q. Yuan, H. P. Jia, J. Zhang and G. Y. Yang, *Chem. Commun.*, 2007, **43**, 1858.
29 J. W. Zhao, C. M. Wang, J. Zhang, S. T. Zheng, Z. H. Li and G. Y. Yang, *Chem. – Eur. J.*, 2008, **14**, 9223.
30 S. T. Zheng, J. Zhang and G. Y. Yang, *Angew. Chem., Int. Ed.*, 2008, **47**, 3909.
31 S. T. Zheng, J. Zhang and G. Y. Yang, *J. Am. Chem. Soc.*, 2010, **132**, 15102.
32 Z. Zhang, Y. L. Wang, H. L. Li, K. N. Sun and G. Y. Yang, *CrystEngComm*, 2019, **21**, 2641–2647.
33 J. W. Zhao, H. P. Jia, J. Zhang, S. T. Zheng and G. Y. Yang, *Chem. – Eur. J.*, 2007, **13**, 10030.
34 Y. Jiang, C. J. Chen, K. Li, L. P. Cui and J. J. Chen, *Chem. Commun.*, 2025, **61**, 4881–4896.
35 Y. X. Zhang, M. C. Zhu, Y. F. Liu, X. Bai, A. G. Zhang, Y. L. Yang, B. Li and S. X. Liu, *New J. Chem.*, 2025, **49**, 4191–4197.
36 C. P. Pradeep, M. F. Misdrahi, F. Y. Li, J. Zhang, L. Xu, D. L. Long, T. B. Liu and L. Cronin, *Angew. Chem., Int. Ed.*, 2009, **48**, 8309.
37 J. Kang, B. B. Xu, Z. H. Peng, X. D. Zhu, Y. G. Wei and D. R. Powell, *Angew. Chem., Int. Ed.*, 2005, **44**, 6902.
38 C. L. Lv, M. Y. Cheng, J. Hao, N. K. N. Rao and Y. Wei, *Polyoxometalates*, 2025, **4**, 9140106.
39 A. Jimbo, C. Li, K. Yonesato, K. Yamaguchi and K. Suzuki, *Dalton Trans.*, 2025, **54**, 8234–8240.
40 I. B. Nahum and R. Neumann, *Chem. Commun.*, 2003, **39**, 2690.
41 F. Odobel, M. Severac, Y. Pellegrin, E. Blart, C. Fosse, C. Cannizzo, C. R. Mayer, K. J. Eliott and A. Harriman, *Chem. – Eur. J.*, 2009, **15**, 3130.

42 Z. W. Wang, Q. Zhao, C. A. Chen, J. J. Sun, H. Lv and G. Y. Yang, *Inorg. Chem.*, 2022, **61**, 7477–7483.
43 A. Ginsberg, *Inorg. Synth.*, 1990, **27**, 108.
44 G. M. Sheldrick, *Acta Crystallogr., Sect. A: Found. Crystallogr.*, 2015, **71**, 3–8.
45 G. M. Sheldrick, *Acta Crystallogr., Sect. C: Struct. Chem.*, 2015, **41**, 3–8.
46 (*a*) CCDC 2403241: Experimental Crystal Structure Determination, 2026, DOI: 10.5517/ccdc.csd.cc2lnrxy; (*b*) CCDC 2404218: Experimental Crystal Structure Determination, 2026, DOI: 10.5517/ccdc.csd.cc2lpsfj.